Electron-impact ionization of the water molecule at large momentum transfer above the double-ionization threshold

D. B. Jones, M. Yamazaki, N. Watanabe, and M. Takahashi*

Institute of Multidisciplinary Research for Advanced Materials, Tohoku University, Sendai 980-8577, Japan

(Received 1 June 2010; revised manuscript received 25 October 2010; published 14 January 2011)

The single and double ionization of the water molecule at large momentum transfer has been studied using a combination of $(e,2e)$ and $(e,3\text{–}1e)$ spectroscopy, with the binding energy spectrum being measured from 0 to 100 eV. The experiment has been performed in the symmetric noncoplanar geometry at an incident electron energy of 2055 eV. In this way we have achieved a large momentum transfer of 9 a.u. In particular, we present an observation of a relatively intense band at around 58 eV. Symmetry-adapted cluster configuration interaction (SAC-CI) general-R calculations for single ionization indicate that the observed band is at least partly generated by a cluster of satellites with small intensities, which predominantly belong to states possessing $^2A_1$ symmetry originating from the mixing of the $(2a_1)^{-1}$ state with two electron processes. Nevertheless, it has been found that the entire spectrum above the lowest double-ionization threshold cannot be understood, even qualitatively, with the SAC-CI calculations. This result suggests that the $(e,3\text{–}1e)$ double-ionization processes have a significant contribution to the observations.

DOI: 10.1103/PhysRevA.83.012704 PACS number(s): 34.80.Gs

I. INTRODUCTION

Ionization spectra have long provided detailed information regarding the electronic structure of atoms and molecules. In particular, ionization-excitation or shake-up processes and double-ionization processes provide a wealth of information about electron correlation in the target, as the simultaneous excitation of two electrons cannot occur without electron correlation effects. Although a large number of photon-impact experiments have given excellent insights into photoionization dynamics [1], the information they could provide concerning electron correlation has often been hidden in the dipole matrix elements. In this respect, electron-impact single- and double-ionization experiments at large momentum transfer are of interest. This is because the target-ion overlap in the single ionization matrix element can be very sensitive to correlations [2,3] and double ionization is expected to provide direct information on the correlated motion of electrons in the target [4–7].

The reader can refer to excellent review articles [2,3,8–15] for electron-impact single-ionization experiments at large momentum transfer or electron momentum spectroscopy (EMS), so here we note briefly electron-impact double ionization at large momentum transfer. To obtain all of the spectroscopic information regarding the target structure from electron-impact double ionization requires kinematically complete $(e,3e)$ spectroscopy [16], where the energies and momenta of all incoming and outgoing electrons are determined. So far, this method has been employed to obtain direct information about target-electron correlation in two experiments; studies at a momentum transfer of 2.3–2.7 a.u. for $Mg(3s)^{-2}$ by El-Marji *et al.* [17] and at 0.8 a.u. for $He(1s)^{-2}$ and $Ar(3p)^{-2}$ by Lahmam-Bennani *et al.* [18]. Both of these studies have presented evidence that the character of the angular distribution of the center of mass of the ejected electron pair alludes to an "initial-state two-electron wave function." However, the general extension of this method beyond these studies has been hampered due mainly to the experimental difficulties in measuring the differential cross section that becomes significantly smaller as the momentum transfer increases.

With practicable experiments in mind, Popov *et al.* [19] proposed a technically more feasible method, $(e,3\text{–}1e)$ spectroscopy [20–24], in which only two of the three outgoing electrons produced by electron-impact double ionization at large momentum transfer are detected and the remaining outgoing electron is left undetected. Bolognesi *et al.* [25] performed the first $(e,3\text{–}1e)$ experiment along this line to examine the angular distribution of $He(1s)^{-2}$. By employing the symmetric coplanar geometry at an incident electron energy of 580 eV, they achieved momentum transfer values in the range 3.2–6.1 a.u. More recently, $(e,3\text{–}1e)$ studies on He at much larger momentum transfer have been conducted both experimentally and theoretically by Watanabe *et al.* [26,27]. In these studies of our research group, the symmetric noncoplanar geometry has been employed at incident electron energies of 2080 and 4260 eV, with momentum transfers of ca. 9 and 12 a.u. being achieved, respectively. Comparisons of the $(e,3\text{–}1e)$ experiments with second-order Born-approximation (SBA) calculations, as well as those employing the first-order plane-wave impulse approximation (PWIA) [28], have shown that the momentum dependence of the experimental results is well reproduced at the PWIA level provided a highly correlated wave function is employed, though there still remains noticeable higher-order effects due to the two-step (TS) mechanisms [29,30] rather than distorted wave effects.

Since the $(e,3\text{–}1e)$ technique has been successful for the two-electron target, one of the next steps may be to extend this method to many-electron targets. However, $(e,3\text{–}1e)$ studies on many-electron targets impose an additional experimental difficulty; ionization-excitation processes can occur above the double-ionization threshold, and they may coexist with double-ionization processes to produce a composite spectrum. In heavier atomic targets, such as Ne [31,32], satellite bands

*masahiko@tagen.tohoku.ac.jp

exhibiting well-defined peak structures above the double-ionization threshold have been well investigated in terms of the shake-up mechanism; however, studies on double ionization are extremely scarce. As such, the understanding of ionization above the double-ionization threshold is still in its infancy, with even the ratio of direct double to single ionization being unknown for all but the He case [33]. Furthermore, to the best of our knowledge, there have been no explicit studies to observe binding energy spectra of molecules at large momentum transfer over extended binding energy ranges where both single- and double-ionization processes occur. Under these circumstances, we have performed a simultaneous $(e,2e)$ and $(e,3\text{–}1e)$ experiments on water over a binding energy range from 0 to 100 eV.

Water is the most abundant molecule on Earth's surface and a major constituent of all living organisms. It is also an important constituent of Earth's atmosphere and is found in many forms throughout the cosmos and general interstellar space. For these reasons, structural and dynamical information about water has been attracting broad interest from a diverse range of studies. Indeed, photoelectron spectroscopy [34–36] and EMS [37–41] have provided an excellent picture of the single ionization of water below the vertical double-ionization threshold (∼39 eV [42]). This has been complemented by years of assiduous effort devoted to studying the double ionization of this molecule, which have included Auger electron spectroscopy [43,44], photoion-photoion coincidence spectroscopy [45], double charge transfer spectroscopy [46], photoelectron-photoelectron coincidence spectroscopy [42], and electron-impact dissociative double-ionization cross-section measurements [47,48]. Nevertheless, to the best of our knowledge there have been no attempts to measure $(e,2e)$ and $(e,3\text{–}1e)$ spectra at large binding energies for this molecule, which may provide highly sensitive information on the correlated motion of electrons. This fact has provided a strong motivation for the present study.

In this paper we report binding energy spectra of water, measured at high precision, over a wide binding energy range from 0 to 100 eV. The experiment has been conducted at an incident electron energy of 2055 eV using a symmetric noncoplanar $(e,2e)$ spectrometer [49] that features high collection efficiency by simultaneously covering wide binding energy and momentum ranges [50]. Here a large momentum transfer of ca. 9 a.u. has been achieved. In this first instance we wish to clarify the contributions of $(e,2e)$ and $(e,3\text{–}1e)$ processes at high binding energy for molecules. To achieve this, the measured spectra, as a function of both energy and momentum, will be discussed with the aid of calculations using the symmetry-adapted cluster configuration interaction (SAC-CI) general-R method [51].

II. EXPERIMENTAL METHOD

For electron-impact single-ionization and double-ionization processes of H_2O, conservation of linear momentum and energy requires:

$$\boldsymbol{p}_{H_2O^+} = \boldsymbol{p}_0 - \boldsymbol{p}_1 - \boldsymbol{p}_2, \tag{1}$$

$$V_i = E_0 - E_1 - E_2, \tag{2}$$

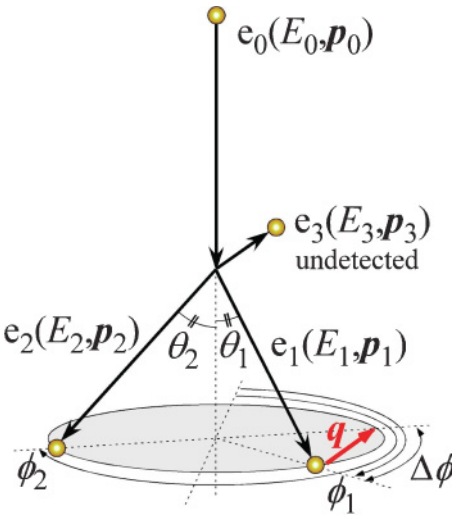

FIG. 1. (Color online) Schematic of the symmetric noncoplanar geometry for the study of $(e,2e)$ and $(e,3\text{–}1e)$ reactions at large momentum transfer.

and

$$\boldsymbol{p}_{H_2O^{2+}} + \boldsymbol{p}_3 = \boldsymbol{p}_0 - \boldsymbol{p}_1 - \boldsymbol{p}_2, \tag{3}$$

$$E_3 + V_i^{2+} = E_0 - E_1 - E_2. \tag{4}$$

Here the $\boldsymbol{p}_j$'s and E_j's $(j = 0,1,2,3)$ are momenta and kinetic energies of the incident and outgoing electrons, respectively. $\boldsymbol{p}_{H_2O^+}$ and $\boldsymbol{p}_{H_2O^{2+}}$ represent the recoil momenta of the residual singly (H_2O^+) and doubly (H_2O^{2+}) charged ions, respectively. Likewise, V_i and V_i^{2+} denote the respective single- and double-ionization potentials of H_2O. Since the present experiment involves the detection of both energy and momenta of two fast outgoing electrons in coincidence, $\boldsymbol{p}_{H_2O^+}$ and V_i are fully determined from Eqs. (1) and (2). In this way an $(e,2e)$ binding energy spectrum can be measured as a function of $\boldsymbol{p}_{H_2O^+}$. On the other hand, for the $(e,3\text{–}1e)$ process $(\boldsymbol{p}_{H_2O^{2+}} + \boldsymbol{p}_3)$ and $(V_i^{2+} + E_3)$ are determined. Thus, an $(e,3\text{–}1e)$ binding energy spectrum can be measured as a function of $(\boldsymbol{p}_{H_2O^{2+}} + \boldsymbol{p}_3)$. For the sake of simplicity, both $\boldsymbol{p}_{H_2O^+}$ in $(e,2e)$ and $(\boldsymbol{p}_{H_2O^{2+}} + \boldsymbol{p}_3)$ in $(e,3\text{–}1e)$ are called momentum $\boldsymbol{q}$ here.

Figure 1 shows a schematic diagram of the symmetric noncoplanar geometry that has been widely used for $(e,2e)$ spectroscopy at large momentum transfer [2,3,6,8–15]. In this kinematic scheme, two outgoing electrons having equal energies $(E_1 = E_2)$ and making equal polar angles $(\theta_1 = \theta_2 = 45^\circ)$ with respect to the incident electron beam direction are detected in coincidence. The magnitude of the momentum q is then expressed by

$$q = \sqrt{(p_0 - \sqrt{2}p_1)^2 + [\sqrt{2}p_1 \sin(\Delta\phi/2)]^2}, \tag{5}$$

where $\Delta\phi$ $(= \phi_2 - \phi_1 - \pi)$ is the out-of-plane azimuthal angle difference between the two outgoing electrons detected. If the incident electron energy E_0 and momentum $\boldsymbol{p}_0$ are fixed, a given ionization transition (V_i) can be selected simply by the choice of detection energy $(E_1 = E_2)$ and then q can be determined only by $\Delta\phi$. The same is also true for $(e,3\text{–}1e)$ experiments, if we detect two fast outgoing electrons with

equal energies in the symmetric noncoplanar geometry while leaving one slow outgoing electron undetected.

In the present work an electron-electron-fragment ion triple coincidence spectrometer [49] has been employed to carry out (e,2e) and (e,3–1e) measurements of water simultaneously. Although the spectrometer has been developed for (e,2e) experiments with fixed-in-space molecules [52], it can be used to produce (e,2e) and (e,3–1e) data by detection of the two fast outgoing electrons only. Details of the spectrometer have been described elsewhere [49], so only a brief summary of the electron experimental aspects is given here. An electron gun incorporating a tungsten filament produces an electron beam of typically 60 μA in the interaction region, as measured with a Faraday cup. The interaction volume is created by the overlap of the electron beam and the target gas, which is introduced by eight gas nozzles. A pair of 0.5-mm apertures restrict the electrons leaving the interaction volume so that only those with polar angles of $\theta = 45^\circ$ and azimuthal angles ϕ_1 and ϕ_2 in the ranges between 70°–110° and 250°–290° are accepted into a spherical analyzer. Note that we have employed here a rather large polar acceptance angle of $\Delta\theta = \pm 1.5^\circ$ in order to achieve a higher collection efficiency, although this deteriorates the obtainable energy and momentum resolutions. The accepted electrons are dispersed, based on their kinetic energies, by the spherical analyzer before being detected by a pair of position-sensitive detectors placed behind an exit aperture. Since a spherical analyzer maintains the azimuthal angles of the electrons, both the energies and the angles can be determined from the arrival positions at the detectors. Thus, by combining a spherical analyzer with a pair of position-sensitive detectors, it is possible to sample the (e,2e) and (e,3–1e) cross sections over a wide range of binding energies ($E_{\rm bind} = E_0 - E_1 - E_2$) and momenta ($q$) in parallel. This technique significantly improves sensitivity and accuracy of the data compared with conventional single-channel measurements, as drifts in electron beam current and fluctuations in target-gas density affect all channels in the same way.

Water (Kanto Chemical Co., Inc. 11307-79) was subjected to repeated freeze-pump-thaw cycles before use. The pure water sample was held in a refrigerated water bath at 10 °C and its vapor was leaked into the interaction region through the eight gas nozzles. The simultaneous (e,2e) and (e,3–1e) experiment was performed at an incident electron energy of 2055 eV, while keeping an ambient sample gas pressure at ca. 3.0×10^{-4} Pa. Two outgoing electrons having energies on the order of 1.0 keV were detected in coincidence. The instrumental energy and momentum resolutions obtained were ca. 4.2 eV full width at half maximum (FWHM) and 0.34 a.u. at $\Delta\phi = 0^\circ$ for the experiment. In this way, experimental results were obtained by accumulating data for 2 months, with no detectable impurities being observed in the binding energy spectra.

III. THEORETICAL BACKGROUND

(e,2e) spectroscopy at large momentum transfer has long been regarded as a probe of molecular orbitals in momentum space [2,3,6,8–15]. A full discussion of the relevant scattering theory can be found in the literature, so we do not repeat those details again here. Briefly, however, within the PWIA the triple differential cross section (TDCS) for (e,2e) single ionization is given by

$$\frac{d^3\sigma_{(e,2e)}}{d\Omega_1 d\Omega_2 dE_1} = (2\pi)^4 \frac{p_1 p_2}{p_0} f_{\rm ee} \times \sum_{\rm av} \left|\left\langle \boldsymbol{p}_2\, \Psi_{\rm f}^{N-1} | e^{{\rm i}(\boldsymbol{p}_0 - \boldsymbol{p}_1)\cdot \boldsymbol{r}_1} | \Psi_{\rm i}^{N} \right\rangle\right|^2. \quad (6)$$

Here $\Psi_{\rm i}^N$ and $\Psi_{\rm f}^{N-1}$ are the N-electron initial neutral and $(N-1)$-electron final ion target wave functions, respectively. $\boldsymbol{r}_1$ denotes the spatial coordinate of the target electron before/after ionization. $\Sigma_{\rm av}$ represents an average over the initial state degeneracies and a sum over the final states that are unresolved in the experiment. For molecular targets, it also involves a spherical average over the random orientations of the gaseous target. The electron-electron collision factor $f_{\rm ee}$ is given [3,53] by

$$f_{\rm ee} = \frac{1}{4\pi^4} \frac{2\pi\eta}{\exp(2\pi\eta) - 1} \left[\frac{1}{|\boldsymbol{p}_0 - \boldsymbol{p}_1|^4} + \frac{1}{|\boldsymbol{p}_0 - \boldsymbol{p}_2|^4} - \frac{1}{|\boldsymbol{p}_0 - \boldsymbol{p}_1|^2} \frac{1}{|\boldsymbol{p}_0 - \boldsymbol{p}_2|^2} \cos\left(\eta \ln \frac{|\boldsymbol{p}_0 - \boldsymbol{p}_2|^2}{|\boldsymbol{p}_0 - \boldsymbol{p}_1|^2} \right) \right], \quad (7)$$

with

$$\eta = \frac{1}{|\boldsymbol{p}_1 - \boldsymbol{p}_2|}. \quad (8)$$

Further, if the (e,2e) reaction takes place so that it is described within the binary encounter approximation [3,8], which assumes a single collision between the incident and target electrons such that there is a clean knockout of the bound electron and the residual ion acts as a spectator, the momentum of the target electron before ionization, $\boldsymbol{p}$, is equal in magnitude but opposite in sign to the ion recoil momentum $\boldsymbol{q}$:

$$\boldsymbol{p} = -\boldsymbol{q} = \boldsymbol{p}_1 + \boldsymbol{p}_2 - \boldsymbol{p}_0. \quad (9)$$

The symmetric noncoplanar geometry employed here is best suited to see (e,2e) reactions under such clean-knockout conditions, where the momentum transfer ($|\boldsymbol{p}_0 - \boldsymbol{p}_1|$) is large and all of the momentum transferred to the target is absorbed by the ejected electron. Using Eq. (9), we obtain

$$\frac{d^3\sigma_{(e,2e)}}{d\Omega_1 d\Omega_2 dE_1} = (2\pi)^4 \frac{p_1 p_2}{p_0} f_{\rm ee} \sum_{\rm av} \left|\left\langle \boldsymbol{p}\ \Psi_{\rm f}^{N-1} \left| \Psi_{\rm i}^{N} \right\rangle\right|^2. \quad (10)$$

The structure factor $|\langle \boldsymbol{p}\ \Psi_{\rm f}^{N-1} | \Psi_{\rm i}^{N} \rangle|^2$ in Eq. (10) is simply the square of the momentum space representation of the quasiparticle or Dyson orbital. While the Dyson orbital can be fully evaluated in a configuration interaction picture, it can often be well approximated, in the weak-coupling approximation [2,3], by the ionized Hartree-Fock (HF) or Kohn-Sham (KS) [54] orbital, $\phi_\alpha(\boldsymbol{p})$, by introducing a spectroscopic factor or pole strength, $S_\alpha^{\rm f}$, such that

$$\left\langle \boldsymbol{p}\ \Psi_{\rm f}^{N-1} \left| \Psi_{\rm i}^{N} \right\rangle = \sqrt{S_\alpha^{\rm f}} \phi_\alpha(\boldsymbol{p}). \quad (11)$$

Within this picture, the spectroscopic factors satisfy the following sum rule:

$$\sum_f S_\alpha^{\rm f} = 1, \quad (12)$$

where the sum runs over all possible final states belonging to the α-symmetry manifold. These are the so-called target HF [3,8] or KS approximations [55–57] and are valid only when the respective HF or KS wave function yields a good description of the initial target state, Ψ_i^N. Using Eq. (11), the final form of the TDCS within the PWIA is

$$\frac{d^3\sigma_{(e,2e)}}{d\Omega_1 d\Omega_2 dE_1} = (2\pi)^4 \frac{p_1 p_2}{p_0} f_{ee} \sum_{\text{av}} S_\alpha^{\text{f}} \left|\phi_\alpha(\boldsymbol{p})\right|^2. \quad (13)$$

Thus, $(e,2e)$ spectroscopy at large momentum transfer enables one to look at electron orbitals in momentum space. This is the underlying reason why the technique is also called EMS.

Likewise, following an extension of the PWIA for $(e,3–1e)$ double ionization of He at large momentum transfer proposed by Popov *et al.* [19] to many electron molecules, we obtain the following fourfold differential cross section (4DCS):

$$\frac{d^4\sigma_{(e,3-1e)}}{d\Omega_1 d\Omega_2 dE_1 dE_3} = (2\pi)^4 \frac{p_1 p_2 p_3}{p_0} f_{ee} \int d\Omega_3 \times \sum_{\text{av}} \left|\left\langle \boldsymbol{p}_2 \Psi_{\text{f},\boldsymbol{p}_3}^{N-1} \middle| e^{i(\boldsymbol{p}_0-\boldsymbol{p}_1)\cdot\boldsymbol{r}_1} \middle| \Psi_{\text{i}}^N \right\rangle\right|^2. \quad (14)$$

Once again, the sum represents an average over the initial states and sum over final state degeneracies, but now there is also an integration over the directions of the undetected electron. $\Psi_{\text{f},\boldsymbol{p}_3}^{N-1}$ is the target's final $(N-1)$-electron wave function having $(N-2)$ bound electrons and one continuum electron with momentum $\boldsymbol{p}_3$. In this case the doubly ionized state is created by the shake-off mechanism [29], where one of the originally bound electrons is simultaneously ejected due to the sudden change in potential originating from the ejection of the first electron.

Finally, it is worthwhile to note the potential information regarding the target's electron correlation obtainable in $(e,3–1e)$ spectroscopy. As previously noted by Popov *et al.* [19], the form of Eq. (14) is comparable to that of the TDCS for $(e,2e)$ single ionization [see Eq. (6)]. However, in this case the structure amplitude is the Fourier transform of the initial state's projection onto a shake-off final state that has $(N-2)$ bound electrons and one continuum electron with momentum $\boldsymbol{p}_3$. While the low energy of the continuum electron requires a complete treatment of its interaction with the doubly charged ion core, it is advantageous to consider the electron as a plane wave and neglect any orbital relaxation upon double ionization. With this simplification, we can see that the structure amplitude reduces to the partial two-electron momentum density, $|\Psi_{\text{if}}^N(\boldsymbol{p},\boldsymbol{p}')|^2$, the absolute square of the projection of the initial-state wave function onto the doubly ionized state in the momentum representation [5]. It is this information regarding the two-electron density, and hence electron correlation, that is only available through the $(e,3–1e)$ contribution. While the ionization-excitation processes provide sensitive information about the target structure in their own right, it is this potential to extract unique information regarding electron correlation from the double-ionization contribution that creates a need to assess the respective contributions of single and double ionization to the spectral intensity at energies above the first double-ionization potential.

In the present work, in order to obtain a qualitative assessment of the contributions from ionization-excitation processes of water to the measured spectra, we have performed SAC-CI general-R calculations [51] using GAUSSIAN 03 [58]. In the calculations, we have used the relatively small augmented correlation consistent valence double-ζ basis set [59], which we have expanded by adding Rydberg functions on the oxygen atom [60]. The included excitation operators have been restricted up to triples.

IV. RESULTS AND DISCUSSION

In Fig. 2 we show representative $(e,2e)$ and $(e,3–1e)$ binding-energy spectra of H_2O obtained concurrently at an impact energy of 2055 eV, which were constructed by plotting the number of true coincidence events detected, after a correction for variations in the detector collection efficiency, as a function of the binding energy (E_{bind}). The binding energy spectra at three specific azimuthal angle differences, $\Delta\phi = 0°$, 6°, and 12°, are shown to illustrate the momentum dependence variation between individual ionization bands. Vertical bars indicate the presently obtained binding energies for single-ionization, as well as double-ionization thresholds reported by

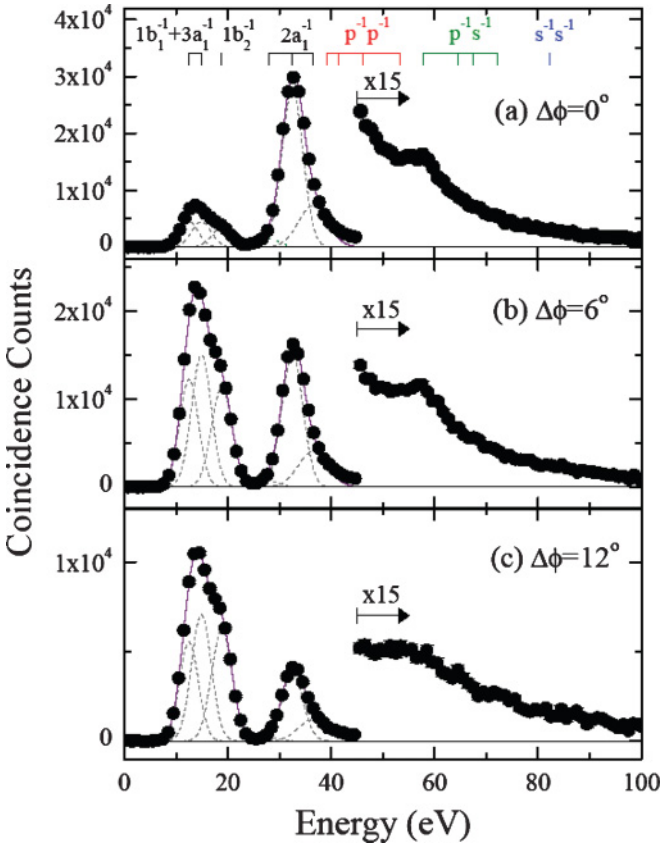

FIG. 2. (Color online) $(e,2e)$ and $(e,3–1e)$ binding energy spectra of H_2O at (a) $\Delta\phi = 0°$, (b) $\Delta\phi = 6°$, and (c) $\Delta\phi = 12°$, obtained at an incident electron energy of 2055 eV. For ease of comparison, the data for binding energy above 45 eV are scaled by a factor of 15. The dashed lines represent fitting curves and the solid lines are their sums. See text for details.

Auger electron spectroscopy [44] and assigned by a Green's function method [61]. Here the observed spectra, in the outer- and inner-valence single-ionization regions ($E_{\text{bind}} <$ ca. 45 eV), are consistent with those of the previous (e,2e) studies [37–41], although the individual outer-valence orbitals cannot be completely resolved with the present experimental energy resolution. Note that in the present study we have opted, at the expense of energy resolution, to achieve higher collection efficiency over a large binding energy range that includes the previously unexplored range from 50 to 100 eV. The spectra in Fig. 2 are now discussed in detail.

First, the outer-valence region of the present spectra reveals one spectral envelope corresponding to the ionization of the three outermost orbitals: $1b_1$,$3a_1$, and $1b_2$. The second prominent feature belongs to the inner-valence $2a_1$ orbital. One can see that this feature is particularly broad, mainly resulting from a significant breakdown of the independent-particle picture [37–41,62]. In order to reproduce the $2a_1$ experimental spectra, a fitting procedure determined the appropriate weights for three Gaussian curves with FWHM of 4.6, 4.8, and 6.7 eV, centered at $E_{\text{bind}} = 28.0$, 32.5, and 36.5 eV, respectively. It is evident from Fig. 2 that the momentum dependence of the (e,2e) cross section is strongly sensitive to the transition in question. Nevertheless, they can be classified from their dominant behavior into two broad categories; s and p type. For instance, the three outermost $1b_1$,$3a_1$, and $1b_2$ orbitals have their maxima in the (e,2e) cross section at nonzero momentum and are hence characterized as p type. On the other hand, the main band ($E_{\text{bind}} = 32.5$ eV) in the $2a_1$ orbital manifold has its maximum intensity at the momentum origin and is thus characterized as s type. Further, the cross sections for the two satellite bands exhibit the same momentum dependence, which is expected from Eq. (13). While in previous higher-resolution experiments more fitting functions have been employed, this intensity is distributed into our broader fitting functions as they share the same momentum dependence. Note that these observations, for $E_{\text{bind}} < 45$ eV, are fully supported by the findings of previous (e,2e) studies [37–41] and validate our present experimental procedure. We can therefore confidently examine the previously unexplored higher-binding-energy region.

For ease of comparison, the binding-energy spectra for $E_{\text{bind}} > 45$ eV are rescaled by a factor of 15 in Fig. 2. In this binding-energy region the spectral intensity is seen to monotonically decrease as the binding energy increases, with the exception being at around $E_{\text{bind}} = 58$ eV, where a broad band having a peaklike structure is clearly observed. Apart from this peak feature, the observed binding-energy spectrum at each $\Delta\phi$ does not exhibit any noticeable structure, although spectral intensity is present across the entire higher-binding-energy range covered. Furthermore, by comparing the spectra at each $\Delta\phi$, we can observe that the maximum of the spectral intensity always lies in the low-momentum region ($\Delta\phi = 0^\circ$). In order to facilitate the interpretation of the present spectra in the first instance, throughout the proceeding sections we limit our discussions to the framework of ionization-excitation processes within the PWIA weak-coupling expansion of the target ion overlap [2,3]. Within this picture this maximum spectral intensity in the low-momentum region indicates a dominant s character. This observation suggests that the s-character $2a_1$ orbital is a major contributor to the spectral intensity.

On the other hand, to gain qualitative insights into the origins of the broad band at around 58 eV, we initially compare the present result to that observed for the isoelectronic Ne atom. For Ne, the satellite bands exhibiting well-defined peak structures have been well studied using both EMS [31,32] and high-energy photoelectron spectroscopy [63]. For instance, two prominent satellite bands at 78.90 and 88.32 eV have been assigned to transitions to the $2s^{-1}2p^{-1}(^3P)3p\,^2S$ and $2s^{-1}2p^{-1}(^1P)3p\,^2S$ states, which belong to Rydberg series that converge to the $2s^{-1}2p^{-1}(^3P)$ and $2s^{-1}2p^{-1}(^1P)$ double-ionization potentials at ~88 and 98 eV [64], respectively. Thus, the observed band at around 58 eV for water is expected to have origins in the series of $p^{-1}s^{-1}np$ states that converge to the known $p^{-1}s^{-1}$ double-ionization potentials. This qualitative assignment appears to be supported by the momentum ($\Delta\phi$) dependence of the observed band presenting with s character, because the momentum dependence of the (e,2e) cross section for a satellite transition is similar to that of the main ionization transition.

A rigorous discussion concerning the assignment of the peak structure can be made with Fig. 3 where a theoretical binding energy spectrum using the monopole intensities [65,66] generated by the SAC-CI general-R calculations is presented. Here the calculated monopole intensities have been convolved with the present experimental energy resolution. For ease in visualizing the higher-binding-energy contributions and comparing with experiment, the calculated spectral intensity has been rescaled by a factor of 15 for binding energies above 45 eV. While the present calculations are quite limited in terms of both the basis set size and excitation operators included, they still provide an excellent description of the primary ionization bands as well as satellites at relatively low binding energies. For instance, the calculated value for the shake-up onset of 27.76 eV is in excellent agreement with experiment [38]. It is therefore expected that the theoretical binding-energy spectra in Fig. 3 provide at least a qualitative interpretation of the behavior in the previously unexplored higher-binding-energy region. Indeed, this spectrum indicates a significant increase in binding-energy spectra at around 58 eV, supporting the assignment to ionization-excitation processes. However, it should be noted that in contrast to the Ne case the resulting feature at 58 eV is due to a cluster of satellites with small intensities that originate from the mixing of the $(2a_1)^{-1}$ state with two-electron processes. Furthermore, some of the major poles include dominant configurations, such as $(3a_1)^{-2}(na_1)$ or $(1b_2)^{-1}(1b_1)^{-1}(na_2)$, suggesting that the observed feature cannot unequivocally be interpreted as a state or series of states converging to the $p^{-1}s^{-1}$ double-ionization potentials.

The SAC-CI result also indicates that the bulk of the single-ionization intensity over the entire high-binding-energy region arises from states possessing $^2A_1$ symmetry. This is particularly true in the vicinity of the peak structure at around 58 eV, where the states of $^2B_1$ and $^2B_2$ symmetry have very small intensities. In this respect, analysis of the one-hole final-state configuration interaction coefficients suggests that the monopole intensity originating from the majority of the $3a_1$ orbital is accounted for in the outer-valence energy region

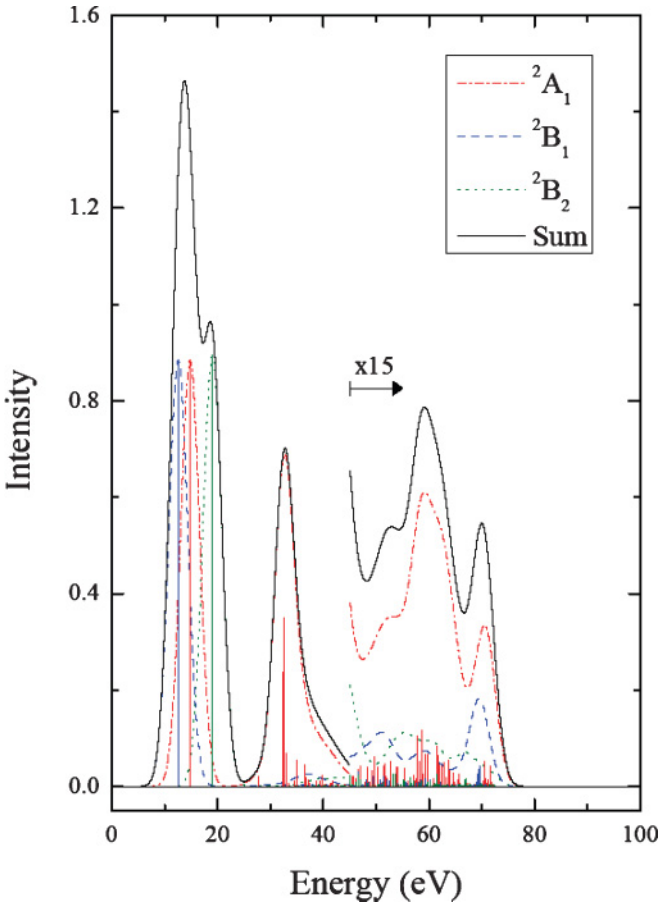

FIG. 3. (Color online) Theoretical binding energy spectra generated by convolving the SAC-CI monopole intensities with the present experimental energy resolution. Also shown are the spectral components for each molecular symmetry. For ease of comparison with the experiment, the calculated values for binding energy above 45 eV are scaled by a factor of 15. See text for details.

and accordingly supports our observation that the *s*-character $2a_1$ orbital is the major source of the spectral intensity over the entire high-binding-energy region. However, the observed experimental momentum dependence is somewhat different from that for the main $2a_1$ profile. Here the main transition decreases more rapidly than the satellite transition with the increase in momentum. This discrepancy suggests that the ionization-excitation processes cannot fully account, within the PWIA target HF or KS approximation, for the experimental behavior.

Moreover, a distinct difference in the spectral intensity distribution of the experiment and SAC-CI calculations is observed. Although the experimental intensity, on the whole, decreases monotonically with the increase in binding energy, the SAC-CI calculations show minima in intensity at around 49 and 67 eV. A possible clue for understanding the difference may be to consider what is obviously lacking in describing the experiment in terms of only the SAC-CI calculations, that is, a contribution from double-ionization processes for transitions to the $p^{-1}p^{-1}$ and $p^{-1}s^{-1}$ states which are accessible in this binding-energy region. Furthermore, the location of minima in the theoretical SAC-CI spectrum not seen experimentally suggests that there is a significant contribution of $(e,3–1e)$ double-ionization processes to the observed binding-energy spectra.

While significant insights have been gained regarding the ionization behavior at high binding energies and large momentum transfer, the present experimental results eagerly await a detailed analysis by sophisticated theoretical calculations. Within the framework of PWIA, the spectral intensity distribution and its momentum dependence should be examined by evaluating the direct overlap of the initial neutral and final ion target wave functions (Dyson orbital) for each single ionization transition, beyond the target HF and KS approximations, by using Green's function and SAC-CI methods including larger basis sets and higher-order excitations. The extension of these methods to $(e,3–1e)$ double ionization is also awaited to account for the observed difference between the experiment and SAC-CI calculations, although such treatments may be challenging. Beyond the first-order PWIA, comparisons with theoretical models including the TS mechanisms in addition to the shake-off mechanism would also be interesting. The recent theoretical approaches using approximate three-Coulomb or Brauner-Briggs-Klar methods to study the double ionization of H_2O at small momentum transfer [67,68] should also be extended to large-momentum-transfer kinematics. Similar $(e,3–1e)$ experiments with higher energy resolution would also be informative and may help to identify individual ionization processes. Work in these directions is already under way in the hope of yielding a more complete description of the ionization process at large momentum transfer and the relative contributions of single and double ionization.

V. SUMMARY

We have presented an $(e,2e)$ and $(e,3–1e)$ spectroscopy study of the ionization of H_2O above the double-ionization threshold. This represents the first extension of $(e,2e)$ spectroscopy of molecules at large momentum transfer over an extended binding energy range spanning multiple double-ionization potentials. A relatively intense band has been observed at around 58 eV, which is at least partly composed of a cluster of small satellites resulting from the $(2a_1)^{-1}$ state mixing with two-electron processes. However, the entire spectrum above the double-ionization threshold cannot be understood, even qualitatively, with the SAC-CI calculations for single ionization. This result suggests that the $(e,3–1e)$ double-ionization processes have a significant contribution to the observations. At the same time, it highlights the need of theoretical assistance to quantitatively obtain insights into the electron-impact ionization of molecules at high binding energies under large-momentum-transfer kinematics.

ACKNOWLEDGMENTS

This research was partially supported by a Grant-in-Aid for Scientific Research (S), Grant No. 20225001 from Japan Society for the Promotion of Science (JSPS) as well as that for JSPS Fellows, Grant No. 20-08762. D.B.J. gratefully acknowledges JSPS for a postdoctoral fellowship.

[1] J. H. D. Eland, Adv. Chem. Phys. **141**, 103 (2009).
[2] I. E. McCarthy and E. Weigold, Rep. Prog. Phys. **54**, 789 (1991).
[3] E. Weigold and I. E. McCarthy, *Electron Momentum Spectroscopy* (Kluwer Academic/Plenum Publishers, New York, 1999).
[4] V. G. Neudatchin, Yu. F. Smirnov, A. V. Pavlitchenkov, and V. G. Levin, Phys. Lett. A **64**, 31 (1977).
[5] Yu. F. Smirnov, A. V. Pavlitchenkov, V. G. Levin, and V. G. Neudatchin, J. Phys. B **11**, 3587 (1978).
[6] V. G. Neudatchin, Yu. V. Popov, and Yu. F. Smirnov, Phys. Usp. **42**, 1017 (1999).
[7] R. W. van Boeyen, N. Watanabe, J. P. Doering, J. H. Moore, and M. A. Coplan, Phys. Rev. Lett. **92**, 223202 (2004).
[8] I. E. McCarthy and E. Weigold, Phys. Rep. **27**, 275 (1976).
[9] C. E. Brion, Int. J. Quantum Chem. **29**, 1397 (1986).
[10] K. T. Leung, in *Theoretical Models of Chemical Bonding*, edited by Z. B. Maksic (Springer-Verlag, Berlin, 1991), Part 3, p. 339.
[11] M. A. Coplan, J. H. Moore, and J. A. Tossell, Z. Naturforsch. **48A**, 358 (1993).
[12] E. Weigold, Z. Naturforsch. **48A**, 371 (1993).
[13] M. A. Coplan, J. H. Moore, and J. P. Doering, Rev. Mod. Phys. **66**, 985 (1994).
[14] C. E. Brion, G. Cooper, Y. Zheng, I. V. Litvinyuk, and I. E. McCarthy, Chem. Phys. **270**, 13 (2001).
[15] M. Takahashi, Bull. Chem. Soc. Jpn. **82**, 751 (2009).
[16] J. Berakdar, A. Lahmam-Bennani, and C. Dal Cappello, Phys. Rep. **374**, 91 (2003).
[17] B. El-Marji, J. P. Doering, J. H. Moore, and M. A. Coplan, Phys. Rev. Lett. **83**, 1574 (1999).
[18] A. Lahmam-Bennani, C. C. Jia, A. Duguet, and L. Avaldi, J. Phys. B **35**, L215 (2002).
[19] Yu. V. Popov, C. Dal Cappello, and K. Kuzakov, J. Phys. B **29**, 5901 (1996).
[20] A. Duguet, C. Dupré, and A. Lahmam-Bennani, J. Phys. B **24**, 675 (1991).
[21] A. Lahmam-Bennani, H. Ehrhardt, C. Dupré, and A. Duguet, J. Phys. B **24**, 3645 (1991).
[22] B. El Marji, A. Duguet, A. Lahmam-Bennani, M. Lecas, and H. F. Wellenstein, J. Phys. B **28**, L733 (1995).
[23] B. El Marji, A. Lahmam-Bennani, A. Duguet, and T. J. Reddish, J. Phys. B **29**, L157 (1996).
[24] A. Lahmam-Bennani, A. Duguet, and S. Roussin, J. Phys. B **35**, L59 (2002).
[25] P. Bolognesi, C. C. Jia, L. Avaldi, A. Lahmam-Bennani, K. A. Kouzakov, and Yu. V. Popov, Phys. Rev. A **67**, 034701 (2003).
[26] N. Watanabe, Y. Khajuria, M. Takahashi, Y. Udagawa, P. S. Vinitsky, Yu. V. Popov, O. Chuluunbaatar, and K. A. Kouzakov, Phys. Rev. A **72**, 032705 (2005).
[27] N. Watanabe, K. A. Kouzakov, Yu. V. Popov, and M. Takahashi, Phys. Rev. A **77**, 032725 (2008).
[28] N. Watanabe, M. Takahashi, Y. Udagawa, K. A. Kouzakov, and Yu. V. Popov, Phys. Rev. A **75**, 052701 (2007).
[29] T. A. Carlson and M. O. Krause, Phys. Rev. **140**, A1057 (1965).
[30] R. J. Tweed, Z. Phys. D **23**, 309 (1992).
[31] O. Samardzic, S. W. Braidwood, E. Weigold, and M. J. Brunger, Phys. Rev. A **48**, 4390 (1993).
[32] N. Watanabe, Y. Khajuria, M. Takahashi, and Y. Udagawa, J. Electron Spectrosc. Relat. Phenom. **142**, 325 (2005).
[33] J. H. McGuire, N. Berrah, R. J. Bartlet, J. A. R. Samson, J. A. Tanis, C. L. Cocke, and A. S. Schlachter, J. Phys. B **28**, 913 (1995).
[34] M. S. Banna, B. H. McQuaide, R. Malutzki, and V. Schmidt, J. Chem. Phys. **84**, 4739 (1986).
[35] C. E. Brion, D. W. Lindle, P. A. Heimann, T. A. Ferrett, M. N. Piancastelli, and D. A. Shirley, Chem. Phys. Lett. **128**, 118 (1986).
[36] S. Y. Truong, A. J. Yencha, A.M. Juarez, S. J. Cavanagh, P. Bolognesi, and G. C. King, Chem. Phys. **355**, 183 (2009).
[37] A. O. Bawagan, C.E. Brion, E. R. Davidson, and D. Feller, Chem. Phys. **113**, 19 (1987).
[38] C. G. Ning, B. Hajgató, Y. R. Huang, S. F. Zhang, K. Liu, Z. H. Luo, S. Knippenberg, J. K. Deng, and M. S. Deleuze, Chem. Phys. **343**, 19 (2008).
[39] A. J. Dixon, S. Dey, I. E. McCarthy, E. Weigold, and G. R. J. Williams, Chem. Phys. **21**, 81 (1977).
[40] R. Cambi, G. Ciullo, A. Sgamellotti, C. E. Brion, J. P. D. Cook, I. E. McCarthy, and E. Weigold, Chem. Phys. **91**, 373 (1984).
[41] A. O. Bawagan, L. Y. Lee, K. T. Leung, and C. E. Brion, Chem. Phys. **99**, 367 (1985).
[42] J. H. D. Eland, Chem. Phys. **323**, 391 (2006).
[43] W. E. Moddeman, T. A. Carlson, M. O. Krause, B. P. Pullen, W. E. Bull, and G. K. Schweitzer, J. Chem. Phys. **55**, 2317 (1971).
[44] H. Siegbahn, L. Asplund, and P. Kelfve, Chem. Phys. Lett. **35**, 330 (1975).
[45] P. J. Richardson, J. H. D. Eland, P. G. Fournier, and D. L. Cooper, J. Chem. Phys. **84**, 3189 (1986).
[46] J. C. Severs, F. M. Harris, S. R. Andrews, and D. E. Parry, Chem. Phys. **175**, 467 (1993).
[47] S. W. J. Scully, J. A. Wyer, V. Senthil, M. B. Shah, and E. C. Montenegro, Phys. Rev. A **73**, 040701(R) (2006).
[48] E. C. Montenegro, S. W. J. Scully, J. A. Wyer, V. Senthil, and M. B. Shah, J. Electron Spectrosc. Relat. Phenom. **155**, 81 (2007).
[49] M. Takahashi, N. Watanabe, Y. Khajuria, K. Nakayama, Y. Udagawa, and J. H. D. Eland, J. Electron Spectrosc. Relat. Phenom. **141**, 83 (2004).
[50] M. Takahashi, Y. Miyake, N. Watanabe, Y. Udagawa, Y. Sakai, and T. Mukoyama, Phys. Rev. Lett. **98**, 013201 (2007).
[51] H. Nakatsuji, Chem. Phys. Lett. **177**, 331 (1991).
[52] M. Takahashi, N. Watanabe, Y. Khajuria, Y. Udagawa, and J. H. D. Eland, Phys. Rev. Lett. **94**, 213202 (2005).
[53] W. F. Ford, Phys. Rev. **133**, B1616 (1964).
[54] W. Kohn and L. J. Sham, Phys. Rev. **140**, A1133 (1965).
[55] P. Duffy, D. P. Chong, M. E. Casida, and D. R. Salahub, Phys. Rev. A **50**, 4707 (1994).
[56] M. E. Casida, Phys. Rev. A **51**, 2005 (1995).
[57] P. Duffy, Can. J. Phys. **74**, 763 (1996).
[58] M. J. Frisch *et al.*, GAUSSIAN 03, Revision B.05, Gaussian Inc., Pittsburgh PA, 2003.
[59] T. H. Dunning Jr., J. Chem. Phys. **90**, 1007 (1989); T. H. Dunning, Basis set obtained from the BASIS SET EXCHANGE v1.2.2, Environmental Molecular Sciences Laboratory Basis Set Library, US Department of Energy, Pacific Northwest Laboratory.
[60] T. H. Dunning Jr. and P. J. Harrison, in *Modern Theoretical Chemistry*, edited by H. F. Schaefer III (Plenum Press, New York, 1977), Vol. 2; Basis set obtained from the BASIS SET EXCHANGE

v1.2.2, Environmental Molecular Sciences Laboratory Basis Set Library, US Department of Energy, Pacific Northwest Laboratory.

[61] F. Tarantelli, A. Tarantelli, A. Sgamellotti, J. Schirmer, and L. S. Cederbaum, J. Chem. Phys. **83**, 4683 (1985).

[62] M. Ehara, M. Ishida, and H. Nakatsuji, J. Chem. Phys. **114**, 8990 (2001).

[63] S. Svensson, B. Eriksson, N. Martensson, G. Wendin, and U. Gelius, J. Electron Spectrosc. Relat. Phenom. **47**, 327 (1988).

[64] T. Kaneyasu, Y. Hikosaka, E. Shigemasa, F. Penent, P. Lablanquie, T. Aoto, and K. Ito, Phys. Rev. A **76**, 012717 (2007).

[65] S. Suzer, S.-T. Lee, and D. A. Shirley, Phys. Rev. A **13**, 1842 (1976).

[66] R. I. Martin and D. A. Shirley, J. Chem. Phys. **64**, 3685 (1976).

[67] I. Kada, A. Mansouri, C. Dal Cappello, P. A. Hervieux, and A. C. Roy, J. Phys. **42**, 025201 (2009).

[68] A. Mansouri, C. Dal Cappello, I. Kada, C. Champion and A. C. Roy, Phys. Lett. A **373**, 3151 (2009).